Growth of Transient Quantum Mechanical Dirac Wave Functions Thru Electric or Magnetic Fields

A. J. Kalinowski*[1]
[1]Consultant
*Corresponding author: East Lyme CT 06333, kalinoaj@aol.com

Abstract: COMSOL is used for obtaining the quantum mechanics wave function $\{\Psi_n(x,y,z,t)\}$ as a solution to the *time dependent* Dirac equations while determining the growth/decay effect of a preexisting magnetic vector potential $\bar{\mathbf{A}}$ field or scalar electric potential ϕ field on the propagating wave function. The probability evaluation of a particle being at a spatial point can be treated by a) the "matrix mechanics formulation" or b) the "wave function formulation". The latter approach is used herein, because it involves solving field PDE's, thus is directly adaptable to COMSOL .

Keywords: Quantum Mechanics, Time Dependent Dirac Equation, Wave Propagation.

1. Introduction

The paper illustrates the use of COMSOL for obtaining the quantum mechanics wave function $\{\Psi_n(x,y,z,t)\}$ (representing *matter waves*) as a solution to the *time dependent* Dirac equations. These equations are employed in particle physics and historically provided the first combined application of quantum mechanics and relativity theory by introducing a four component wave function $\{\Psi_n\}$, n=1,..4. Historically, $\{\Psi_n\}$ described the behavior of fermion type particles (e.g., electrons) and further predicted the existence of antiparticles (e.g., positrons) even before they were observed experimentally. COMSOL® Usage: the *General-Form PDE* "*time dependent*" study is employed. Archive Refs. [1-3] solve for Quantum Mechanics Dirac wave functions; however, this is the first COMSOL application towards solving the *time dependent* Dirac equations for particles in the presence of a pre-existing magnetic or electric field. It is an extension of Ref.[3] that treated solutions in the electric or magnetic influenced time independent exp(-iωt) SS (Steady State) case.

2. Governing Equations/Theory

Governing equations for the behavior of a free fermion particle of mass $\mathbf{m}$ in the presence of a magnetic and electric field, are represented by the *time dependent* quantum mechanics Dirac equations (with wave functions $\{\Psi_n(x,y,z,t)\}$ as the dependent variables) and are given by [4]:

$$\begin{aligned}
&\frac{1}{c}\frac{\partial\Psi_1}{\partial t}+\frac{\partial\Psi_4}{\partial x}-i\frac{\partial\Psi_4}{\partial y}+\frac{\partial\Psi_3}{\partial z}+i\Psi_1(\Phi+M)\\
&+i(i\mathbf{A}_y\Psi_4-\mathbf{A}_z\Psi_3-\mathbf{A}_x\Psi_4)=0\\
&\frac{1}{c}\frac{\partial\Psi_2}{\partial t}+\frac{\partial\Psi_3}{\partial x}+i\frac{\partial\Psi_3}{\partial y}-\frac{\partial\Psi_4}{\partial z}+i\Psi_2(\Phi+M)\\
&+i(A_z\Psi_4-\mathbf{A}_x\Psi_3-i\mathbf{A}_y\Psi_3)=0 \qquad (1)\\
&\frac{1}{c}\frac{\partial\Psi_3}{\partial t}+\frac{\partial\Psi_2}{\partial x}-i\frac{\partial\Psi_2}{\partial y}+\frac{\partial\Psi_1}{\partial z}+i\Psi_3(\Phi-M)\\
&+i(i\mathbf{A}_y\Psi_2-\mathbf{A}_z\Psi_1-\mathbf{A}_x\Psi_2)=0\\
&\frac{1}{c}\frac{\partial\Psi_4}{\partial t}+\frac{\partial\Psi_1}{\partial x}+i\frac{\partial\Psi_1}{\partial y}-\frac{\partial\Psi_2}{\partial z}+i\Psi_4(\Phi-M)\\
&+i(\mathbf{A}_z\Psi_2-\mathbf{A}_x\Psi_1-i\mathbf{A}_y\Psi_1)=0
\end{aligned}$$

where $\mathbf{m}$=particle mass, c= light speed , $\mathbf{e}$=particle charge, $\hbar$ =h/(2π), (*h* is Planck's constant), $i=\sqrt{(-1)}$.

$$\begin{aligned}
&with \quad \mathbf{A}_x\equiv A_x\mathbf{e}/\hbar \quad \mathbf{A}_y\equiv A_y\mathbf{e}/\hbar \quad \mathbf{A}_z\equiv A_z\mathbf{e}/\hbar \qquad (2)\\
&M\equiv \mathbf{m}c/\hbar \quad \Phi\equiv \mathbf{e}\phi/(c\hbar) \quad \bar{\mathbf{B}}=\bar{\nabla}\times\bar{\mathbf{A}} \quad \bar{\mathbf{E}}=-\bar{\nabla}(\Phi)
\end{aligned}$$

Equations(2) relate the normalized vector potential $\bar{\mathbf{A}}$ and scalar potential Φ to the unnormalized vector magnetic $\bar{\mathbf{B}}$ field and electric $\bar{\mathbf{E}}$ field ($\bar{A}$ & ϕ are unnormalized).

2.1 Two-D *time dependen*t form

A 2-D form of governing Eqs.(1) are solved in *time dependent* problems using the COMSOL MULTIPHYSICS® General-Form PDE "T*ime dependent*" studies option. Two dimensional solutions are sought where the wave function depends on spatial coordinates x,y. Thus setting A_z=0 and letting Ψ_n gradients in the z direction drop out, leads to the 2-D form of Eqs.(1) which are the following pair of pde's Eqs.(4a-b) and pair Eqs.(5a-b). In Eqs.(4a-b) and Eqs.(5a-b), nice sized quantities are experienced during the computation process, by using *primed* non-dimensional independent variables and corresponding PDE parameters, as defined by Eqs.(3). The selection of scale values for $\{\mathbf{T},\mathbf{L}\}$ is

treated later in **2.4**. The Eqs.(4a-b) in terms of $\{\Psi_1(x',y',t'),\Psi_4(x',y',t')\}$ *are uncoupled* from the

$$t' \equiv t/\mathbf{T},\ x' \equiv x/\mathbf{L},\ y' \equiv y/\mathbf{L},\ c' \equiv c\mathbf{T}/\mathbf{L},\ \bar{\mathbf{A}}' \equiv \bar{\mathbf{A}}\mathbf{L},\ \bar{\mathbf{E}}' \equiv \bar{\mathbf{E}}\mathbf{L}^2$$
$$M' \equiv M\mathbf{L},\ \omega' \equiv \omega\mathbf{T},\ \Phi' \equiv \Phi\mathbf{L},\ \mathcal{A}' \equiv \mathcal{A}\mathbf{L},\ \bar{\mathbf{B}}' \equiv \bar{\mathbf{B}}\mathbf{L}^2 \quad (3)$$

Eqs.(5a-b) that are in terms of $\{\Psi_2,\Psi_3\}$. Except for the M′ sign, Eq.(4a) is just like Eq.(5a) and Eq. (4b) is just like Eq.(5b) (where $\Psi_1 \leftrightarrow \Psi_3$, $\Psi_4 \leftrightarrow \Psi_2$.

Thus the solution procedure for solving

$$\frac{1}{c'}\frac{\partial\Psi_1}{\partial t'}+\frac{\partial\Psi_4}{\partial x'}-i\frac{\partial\Psi_4}{\partial y'}+i(\Phi'+M')\Psi_1-i\mathcal{A}'^*\Psi_4=0 \quad (4a)$$
$$\frac{1}{c'}\frac{\partial\Psi_4}{\partial t'}+\frac{\partial\Psi_1}{\partial x'}+i\frac{\partial\Psi_1}{\partial y'}+i(\Phi'-M')\Psi_4-i\mathcal{A}'\Psi_1=0 \quad (4b)$$
$$\frac{1}{c'}\frac{\partial\Psi_3}{\partial t'}+\frac{\partial\Psi_2}{\partial x'}-i\frac{\partial\Psi_2}{\partial y'}+i(\Phi'-M')\Psi_3-i\mathcal{A}'^*\Psi_2=0 \quad (5a)$$
$$\frac{1}{c'}\frac{\partial\Psi_2}{\partial t'}+\frac{\partial\Psi_3}{\partial x'}+i\frac{\partial\Psi_3}{\partial y'}+i(\Phi'+M')\Psi_2-i\mathcal{A}'\Psi_3=0 \quad (5b)$$
$$where\ \mathcal{A}'(x,y) \equiv \mathbf{A}'_x+i\mathbf{A}'_y\ ;\quad \mathcal{A}'^*(x,y) \equiv \mathbf{A}'_x-i\mathbf{A}'_y \quad (6)$$

Eqs(4a-b) are just like solving Eqs.(5a-b), thus we focus on solving $\{\Psi_1(x',y',t'),\Psi_4(x',y',t')\}$except for the later Fig.(3) $\{\Psi_3(x',y',t'),\Psi_2(x',y',t')\}$solution example.

2.2 Governing equations in presence of electric potential Φ' field alone ($\bar{\mathbf{A}}'=0$)

In Ref.[3], the steady state *time independent* form Eqs.(4a-b) were solved as one uncoupled PDE for Ψ_1 after algebraically eliminating Ψ_4, where Ψ_4 was later computed by back substitution. A direct coupled approach is used herein (the uncoupled elimination was not possible for the time dependent equations). An alternate form of simultaneous Eqs.(4a-b) is shown in Eqs.(7a-b).

$$\frac{\partial^2\Psi_1}{\partial x'^2}+\frac{\partial^2\Psi_1}{\partial y'^2}-\frac{1}{c'^2}\frac{\partial^2\Psi_1}{\partial t'^2}-2i\frac{\Phi'}{c'}\frac{\partial\Psi_1}{\partial t'}$$
$$+(\Phi'^2-M'^2)\Psi_1+i\left(\frac{\partial\Phi'}{\partial x'}-i\frac{\partial\Phi'}{\partial y'}\right)\Psi_4=0 \quad (7a)$$

$$\frac{\partial^2\Psi_4}{\partial x'^2}+\frac{\partial^2\Psi_4}{\partial y'^2}-\frac{1}{c'^2}\frac{\partial^2\Psi_4}{\partial t'^2}-2i\frac{\Phi'}{c'}\frac{\partial\Psi_4}{\partial t'}$$
$$+(\Phi'^2-M'^2)\Psi_4+i\left(\frac{\partial\Phi'}{\partial x'}+i\frac{\partial\Phi'}{\partial y'}\right)\Psi_1=0 \quad (7b)$$

After setting $\mathcal{A}'=0$, the Eq.(7a) is obtained by first summing $-i\partial/\partial y'$ of Eq.(4b) + $\partial/\partial x'$ of Eq(4b) and then using Eq.(4a) to eliminate the [$\partial\Psi_4/\partial x' - i\partial\Psi_4/\partial y'$] term in that sum. Equation (7b) is obtained by similarly operating on Eq.(4a). Alternate Eqs.(7a-b) have some advantages over Eqs.(4a-b), namely: a) the underlying wave propagation nature of these equations is evident via the embedded classical wave equation appearing in the first three terms, b) they appeared more computationally stable over long time integration histories, c) ease of applying normal derivative boundary conditions (e.g. those found in zero gradient boundary conditions or in absorbing boundary b.c.'s), and d) unlike Eqs.(4a-b) these equations are uncoupled when the electric potential is not present ($\Phi'=0$), where then, each one takes on the form of the relativistic Klein-Gordon Eqs.

Electric Φ' potential selection: The Eq.(8a) scalar potential is selected, and after substituting it into the primed seventh of Eqs.(2), gives the corresponding Eq.(8b) electric field vector $\bar{\mathbf{E}}'$:

$$\Phi' = -(x'-x'_0)\mathbf{E}'_0\ ;\ with \quad \mathbf{E}'_0 = const. \quad (8a)$$
$$\mathbf{E}'_x = \mathbf{E}'_0\ ;\ \mathbf{E}'_y = 0;\ \mathbf{E}'_z = 0 \quad (8b)$$

where x_0' is the offset distance defining the start of the electric field. The size of $\mathbf{E}'_0$ is selected large enough to feel the influence of the electric field on $\Psi_1(x',y',t')$ yet small enough to allow the wave function solution to continue on as a propagating wave and is given by the following Eq.(9) :

$$\mathbf{E}'_0 = \alpha_E k'_D \quad (9)\ ;\quad k'^2_\phi = k'^2_D + \Phi'^2 - 2(\omega'/c')\Phi' \quad (10a);$$
$$k'_D = \sqrt{(\omega'/c')^2 - M'^2} \quad (10b)$$

where Eq.(10b) k'_D is the free field Dirac plane wave *wave number,* α_E is a user picked scale factor, ω' is the frequency of the boundary driven surface used in later example solutions and k'_ϕ is an approximation for a traveling PW *wave number* used later. The reader is referred to Ref.[3] for details on the rationale behind Eqs.(9) and (10a).

2.3 Governing equations in presence of magnetic potential $\bar{\mathbf{A}}'$ field alone ($\Phi'=0$)

A similar direct coupled approach like used in **2.2** is used herein. After setting $\Phi'=0$, the Eq.(11a)

$$\frac{\partial^2\Psi_1}{\partial x'^2}+\frac{\partial^2\Psi_1}{\partial y'^2}-\frac{1}{c'^2}\frac{\partial^2\Psi_1}{\partial t'^2}+i\frac{\mathcal{A}'^*}{c'}\frac{\partial\Psi_4}{\partial t'}-\mathcal{A}'\left(i\frac{\partial\Psi_1}{\partial x'}+\frac{\partial\Psi_1}{\partial y'}\right)$$
$$-\left(i\frac{\partial\mathcal{A}'}{\partial x'}+\frac{\partial\mathcal{A}'}{\partial y'}+M'^2\right)\Psi_1+M'\mathcal{A}'^*\Psi_4=0 \quad (11a)$$

$$\frac{\partial^2\Psi_4}{\partial x'^2}+\frac{\partial^2\Psi_4}{\partial y'^2}-\frac{1}{c'^2}\frac{\partial^2\Psi_4}{\partial t'^2}+i\frac{\mathcal{A}'}{c'}\frac{\partial\Psi_1}{\partial t'}-\mathcal{A}'^*\left(i\frac{\partial\Psi_4}{\partial x'}-\frac{\partial\Psi_4}{\partial y'}\right)$$
$$-\left(i\frac{\partial\mathcal{A}'^*}{\partial x'}-\frac{\partial\mathcal{A}'^*}{\partial y'}+M'^2\right)\Psi_4-M'\mathcal{A}'\Psi_1=0 \quad (11b)$$

is obtained by first summing $-i\partial/\partial y'$ of Eq.(4b) + $\partial/\partial x'$ of Eq.(4b) and then using Eq.(4a) to eliminate the [$\partial\Psi_4/\partial x' - i\partial\Psi_4/\partial y'$] term in that sum. Equation (11b) is obtained by similarly operating on Eq.(4a).

Magnetic $\bar{\mathbf{A}}'$ potential selection: A vector potential is selected given by Eqs.(12a), and

substituting it into the 6th of Eqs.(2), gives the corresponding Eqs.(12b) for the magnetic field $\vec{\mathbf{B}}$:

$$\mathbf{A}'_x = 0;\ \mathbf{A}'_y = (x' - x'_0)\mathbf{B}'_0;\ \mathbf{A}'_z = 0 \ \ with\ \mathbf{B}'_0 = const. \quad (12a)$$

$$\mathbf{B}'_x = 0;\ \mathbf{B}'_y = 0;\ \mathbf{B}'_z = \mathbf{B}'_0 \quad (12b)$$

$$\mathbf{B}'_0 = \alpha_B k'_D \quad (13a); \quad k'^2_{\mathcal{A}} = k'^2_D - |\mathcal{A}'|^2 - \frac{\partial \mathcal{A}'}{\partial y'} - i\frac{\partial \mathcal{A}'}{\partial x'} \quad (13b)$$

where x_0' is the offset distance defining the start of the magnetic field. The size of $\mathbf{B}'_0$ is selected large enough to feel the influence of the magnetic field on $\Psi_1(x',y',t')$, yet small enough to allow the wave function solution to continue as a propagating wave and is given by the Eq.(13a) relationship, where k'_D (given by Eq.(10b)), is the free field Dirac plane wave *wave number,* α_B is a user picked scale factor, ω′ is the frequency of the boundary driven surface used in the example solutions and $k'^2_{\mathcal{A}}$ is an approximation for the traveling wave *wave number* used later. The reader is referred to Ref.[3] for details on the rationale behind Eq.(13a-b).

2.4 Selection of drive frequency ω and non-dimensionalization parameters {T,L}

Frequency selection: De Broglie's photon-to-particle extension of Planck's relation between particle energy E_p and angular frequency ω (i.e. $E_p = \hbar\omega$), along with the *relativistic* relation between E_p and velocity [4], $E_p = mc^2/\sqrt{(1-\beta^2)}$, gives:

$$\omega = \frac{E_p}{\hbar} = cM/\sqrt{1-\beta^2}\ ; \qquad \beta = v_p/c \qquad (14)$$

for selecting the particle frequency in terms of the particle velocity v_p via the speed parameter $\beta = v_p/c$.

Non-dimensionalization {T,L} selection: The scale of the solution domain is such that the numerical size of both time and space variables are extremely small in say standard CGS units. Equations (4a-b), in the non-dimensional prime variables, are valid for *any* unit consistent values of {T,L}, however a convenient choice is to use the time period T_p and wave length λ_D of a propagating Dirac Equation plane wave (in the absence of magnetic or electric fields). The size of all of the *primed variables* in the FEM models (both in model building, solving, and post processing) are then nice size numbers. Equation (15) represents the SS (steady state) representation of the wave

$$\Psi_n(x,y,t) = \psi_n(x,y,\omega)e^{-i\omega t} \quad n = 1;4 \qquad (15)$$

functions where the SS exact solution to *unprimed* Eqs.(4a-b), for a plane wave (inclined θ_{inc} to the x axis, of frequency ω, and traveling in unit vector direction $\vec{n}$, with position vector $\vec{r} = x\vec{i} + y\vec{j}$), is given by Eqs.(16-17) Ref.[4]):

$$\begin{Bmatrix}\psi_1\\ \psi_4\end{Bmatrix} = A\left\{\frac{1}{R}\right\}exp[i\theta_{inc}]\,exp[ik_D\hat{\rho}] \quad ;\hat{\rho} = \vec{n}\cdot\vec{r} \quad (16)$$

$$k_D = \sqrt{(\omega/c)^2 - M^2}\ ;\ R = \frac{k_D}{(\omega/c) - M} \qquad (17)$$

where A is an arbitrary constant. As an example, for a plane wave traveling in the +x direction, set $\vec{n} = +\vec{i}$, θ_{inc}=0, thus $\rho\hat{}$=x; whereas for a wave in the -x direction, set $\vec{n} = -\vec{i}$, θ_{inc}=π, thus $\rho\hat{}$=-x.

Therefore after selecting driver frequency ω, the following scale values for {T,L}are defined by:

$$\mathbf{T} = 2\pi/\omega \quad \mathbf{L} = 2\pi/k_D = 2\pi/\sqrt{(\omega/c)^2 - M^2} \qquad (18a)$$

$$\text{and primed } \omega', k'_D \text{ are: } \omega' = \omega\mathbf{T} \quad k'_D = k_D\mathbf{L} \qquad (18b)$$

3. Method

A finite bounded magnetic or electric field is embedded in a larger domain where the startup zone has a zero magnetic or electric field. This is accomplished by applying COMSOL's "*STEP* functions" (with gradual cubic ∫ shaped rise) to the $\mathbf{B}'_0$ and $\mathbf{E}'_0$ terms (via $\mathcal{A}'$ and Φ′) that appear in Eqs.(4a-b), Eqs.(5a-b), Eqs.(7a-b), and Eqs.(11a-b). The Dirac equation problems are solved in the time domain by driving an upfield face of a model (that is initially at a zero wave function state) with exp(-iω′t′) harmonic loadings, and then track the ensuing transient waves that propagate towards the downfield end of the model.

3.1 FEM Boundary Conditions

3.1.1 FEM Wave Generation Driven Surface: transient solutions are generated by driving the upfield surfaces with time harmonic loadings of the form:

$$\Psi_n(x'_s,y'_s,t') = \psi_n(x'_s,y'_s)f(t')e^{-i\omega' t'}\ n = 1,4 \qquad (19)$$

where $f(t')$ is a gradual time increasing multiplier on the harmonic driver and $\psi_n(x'_s,y'_s)$ is the wave function distribution (from a free field PW or CylW) at surface points $\{x'_s,y'_s\}$. This gradual increase is to help minimize any suddenly applied

$$f(t') = U_2(t')[U_3(t') + U_4(t')\exp(\alpha'(t' - t'_c))] \quad (20)$$

$$U_3(t') = 0 \ \ t' < t'_c\ ; = 1/2 \ \ t' = t'_c\ ; \ = 1 \ \ t' > t'_c$$

$$U_4(t') = 1 \ \ t' < t'_c\ ; = 1/2 \ \ t' = t'_c\ ; \ = 0 \ \ t' > t'_c$$

$$U_2(t') = 0\ t' < 0 \ ; = 2\frac{t'^2}{t'^2_w}\left[\frac{3}{2} - \frac{t'}{t'_w}\right] \ 0 \le t' \le t'_w\ ;$$

$$= 1\ t' > t'_w$$

loading effects. Specifically, the $f(t')$ is given by Eq.(20) with, for example, shaping parameters of :

$$\alpha' = -\ln(\varepsilon_0)/t'_c \; ; \quad t'_c = N_c = 6; \; \varepsilon_0 = .05 \; ; \; t'_w = .1 \quad (21)$$

Firstly $f(t')$ exponentially increases from ε_0 to 1.0 over N_c time cycles (the [ ] bracket term in first of Eqs.(20)). Using transition term $U_2(t')$, the starting value, $f(0) = \varepsilon_0$, is made zero by blending $f(0)=0$ into $f(t'_w)$ with a cubic $\int$ *shaped* curve ending at $t'=t'_w$. The Ψ_1 input driver, using the Eq.(21) parameters, is shown in Fig.(1a) (Ψ_4 is a similar shape). In Fig.(1b), the FFT of the real part of the Ψ_1 driver shows a dominant primed frequency at f′=1.0 .

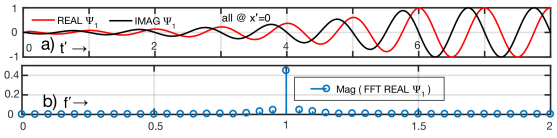

Figure 1. FEM Wave Generation Driver (Ψ_1)

3.1.2 FEM Model Termination Surfaces:

(i) absorbing B.C. : not used; the computations are halted just before the wave meets the outer boundary.

(ii) zero value B.C. : this is used down field of the propagation at the outer boundary points $\{x_b', y_b'\}$ of the model, namely $\Psi_n(x_b', y_b', t') = 0$

(iii) normal gradient B.C. : normal gradient $\vec{n} \bullet \nabla \Psi_n(x'_b, y'_b, t') = 0$, at surface points $\{x_b', y_b'\}$, where $\vec{n}$ is a unit normal vector to the surface and used with Eqs.(7) at wave guide transverse cuts.

(iv) periodic B.C. : $\Psi_n(x', y_b', t) = \Psi_n(x', y_b' + Y', t)$, used with Eqs.(4-5) at two wave guide surfaces Y′ apart.

3.2 FEM Initial Conditions

The FEM model is started from rest throughout the entire spatial domain $\mathcal{D}$, therefore:

$$\Psi_n(x', y', 0) = 0 \; ; \; \frac{\partial \Psi_n(x', y', 0)}{\partial t'} = 0 \; \; all \; x', y' \; in \; \mathcal{D} \quad (22)$$

It is noted that because of the manner Eq.(19) is constructed, evaluating it at $t'=0$ is consistent with Eqs.(22) for both $\Psi_n(x'_s, y'_s, 0)$ and $\partial \Psi_n(x'_s, y'_s, 0)/\partial t'$.

3.3 Probability Computation

The wave functions $\{\Psi_1(x', y', t'), \Psi_4(x', y', t')\}$ can be used to compute the probability $P_{\Delta A}$ of a particle being in a finite area zone, $\Delta A'$, of space for 2-D models. The probability density $\rho(x', y', t')$ is defined as the probability per unit area of the particle being at a particular spatial point $\{x', y'\}$, and is given by Eq.(23) Ref.[4]. The probability $P_{\Delta A}$, can be computed with Eq.(24), where the normalizing factor Λ is set so $P_{\Delta A} \rightarrow 1$ when $\Delta A' \rightarrow A'_{Total}$ (model total area). We compute only $\rho(x', y', t')$.

$$\rho(x', y', \omega') = |\Psi_1|^2 + |\Psi_4|^2 \quad (23)$$

$$P_{\Delta A'} = \Lambda \iint_{\Delta A'} \rho(x', y', t') \, dx' dy' \quad (24)$$

3.4 Model Parameters

All Dirac equation solutions herein use the following parameters in the PDE's: c= 2.998e10 cm/sec, $\hbar = h/(2\pi)$ = 1.055e-27 erg-sec and the particle (electron) mass m = 9.109e-28 grams. Since these parameters are fixed from problem to problem, the Eq.(14) unprimed drive frequency ω is then governed by the remaining particle speed parameter β in all models. Electromagnetic variables are selected via the parameters α_E and α_B and are specified on a per problem basis.

4. Electric Potential Φ' Field Alone ($\bar{A}' = 0$) Results

The basic building blocks of the Dirac theory are freely propagating matter waves such as planar ones. Exact validation solutions to these wave propagation problems (when the spatial varying Φ' potential is present) are not generally possible, even for simple 1-D propagation. Instead COMSOL comparisons to the same problem solved by alternate FEM code (e.g. Mathematica™) is made.

4.1 Bar Plane Wave Guide in Φ' Field

4.1.1 $\{\Psi_1, \Psi_4\}$ *FEM Model Solution* $\mathcal{E}'_0 < 0$:

A W′xL′=4x50 FEM 2-D bar (see Fig.(2b) inset) is driven on the upfield end surface by a uniform load-

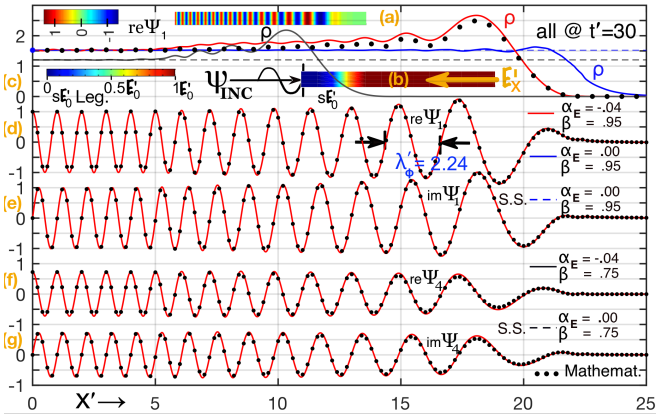

Figure 2. $\{\Psi_1, \Psi_4\}$ PW Passes Thru ($\alpha_E = -0.04$) Φ' Field

ing (with A=1) via Eq.(16) into Eq(19) (e.g. Fig. (1) driver) while using the **3.4** model parameters. The downfield surface is terminated with zero (*ii*)

B.C. and wave guide transverse surfaces use a (*iii*) $\bar{n}\bullet\bar{\nabla}\psi_n(x's,y's)=0$ B.C. . The FEM model consist of three zones: (a) startup *free field* zone where $\mathcal{E}'_0 = 0$; (b) downfield core zone where electric field $\mathcal{E}'_0$ = constant; and (c) transition zones where $\mathcal{E}'_0$ gradually increases between the (a↔b) zones. This is accomplished by multiplying $\mathcal{E}'_0$ in Eq.(8a) with $s(x'-x'_o)*\mathcal{E}'_0$ where s is the appropriately shifted COMSOL built in step function with cubic $\int$ shaped transition zones. The inset in Fig.(2b) shows the resulting $s*\mathcal{E}'_0$ electric field, where dark navy blue is the free field zone, dark red is the constant central core and the rainbow colors in-between show the transition zone. A $x'_o = 3$ shift value is used, which defines the starting point of the electric field $\int$ transition . The Eqs.(7a-b) are solved in COMSOL using the *General-Form PDE "time dependent"* module. The Fig.(2) solutions are at a time snapshot t′=30 and the relevant β frequency and α_E electric field strength parameters are labeled on each plot item. Figure(2c) illustrates the growth of the probability density ρ with $\mathcal{E}'_0$ *turned on vs off*. The Figs.(2d-g) show the growth of the individual $\Psi_1(x'),\Psi_4(x')$ functions where an increasing wavelength vs x′ is observed and cross comparison to a Mathematica FEM solution is good. Figure(2a) is a carpet plot of the Fig.(2d) centerline plot. The wave length (e.g. using Eq.(10a) evaluated @ the mid point x′=15.46 between nulls) is approximated with $\lambda'_\phi \approx 2\pi/k'_\phi = 2.24$ as compared to the Fig.(2d) 2.24 graphical measurement.

4.1.2 $\{\Psi_3,\Psi_2\}$ *FEM Model Solution* $\mathcal{E}'_0 < 0$:

Like the last example except Eqs(5a-b) are solved for $\{\Psi_3,\Psi_2\}$, while using Eq.(16) upfield driver with substitutions: M→ -M, A→R/exp(iθ), $\Psi_1\rightarrow\Psi_3$, $\Psi_4\rightarrow\Psi_2$.

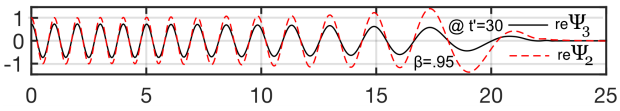

Figure 3. $\{\Psi_3,\Psi_2\}$ PW Passes Thru (α_E = -0.04) Φ′ Field

4.1.3 $\{\Psi_1,\Psi_4\}$ *FEM Model Solution* $\mathcal{E}'_0 > 0$:

The same Fig.(2) model is solved except here $\mathcal{E}'_0 > 0$ thus the Electric field component is in the same direction as the wave propagation. The Figs.(4d-g) show the growth (reduction here) of the individual $\Psi_1(x'),\Psi_4(x')$ functions where a *decreasing wavelength* vs x′ is observed and the cross comparison to Mathematica FEM solution is good. Figure (4a) is a carpet plot of the Fig.(4d) centerline plot. The wave length (e.g. using Eq.(10a) evaluated @ the mid point x′=19.42 between nulls) is approximated with $\lambda'_\phi \approx 2\pi/k'_\phi = 0.596$ as compared to the Fig.(4d) 0.590 graphical measurement.

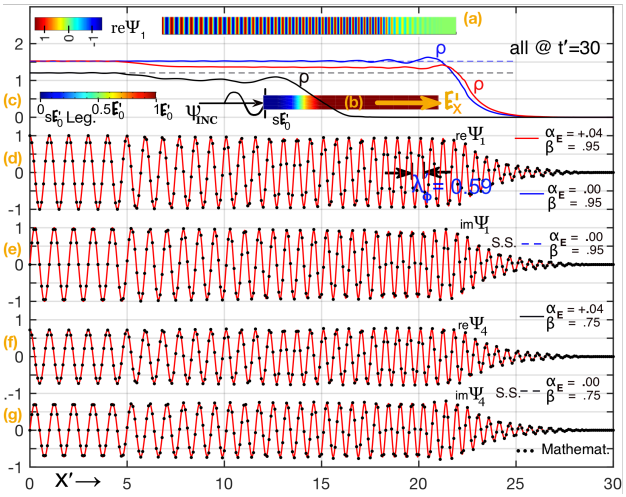

Figure 4. PW Passes Thru (α_E = +0.04) Φ′ Field

4.2 Disk Cylindrical Wave in Φ′ Field

A $(R'_o\text{-}R'_i)x\Theta = (16\text{-}4)x360^o$ FEM 2-D annular

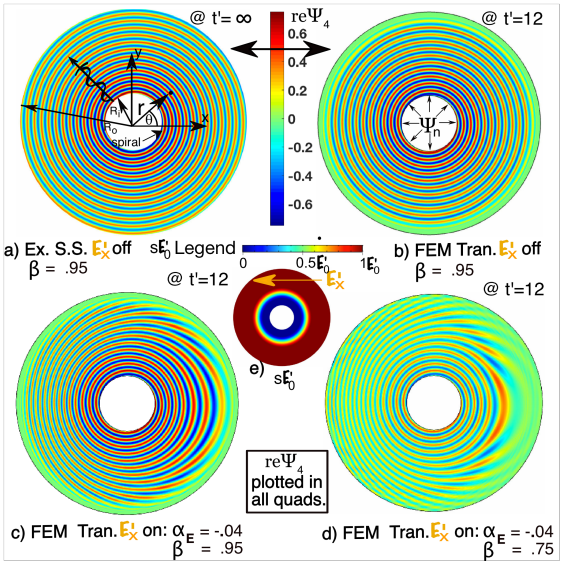

Figure 5. CylW Passes Thru (α_E = -0.04) Φ′ Field

region (e.g. Fig.(5a)) is driven at the inner surface with Eq.(19) while using the Eq(25) Ref.[2] freely

$$\begin{Bmatrix}\psi_1\\ \psi_4\end{Bmatrix} \approx \begin{Bmatrix}1\\ \dfrac{exp[i\theta]}{R'}\end{Bmatrix} \dfrac{exp[ik'_D(r'-R'_i)]}{\sqrt{(r'/R'_i)}} \qquad (25)$$

propagating cylindrical Dirac wave (in {r′,θ}

cylindrical coordinates @ r′=R′$_i$) for the ψ_n amplitudes along with the **3.4** model parameters. The gradual $\mathbf{E}'_0$ *buildup* is accomplished by multiplying $\mathbf{E}'_0$ in Eq.(8a) with $s(r'-r'_o)*\mathbf{E}'_0$ (e.g. Fig.(5e)). Figures(5a-b) give a "$\mathbf{E}'_x$ off" comparison between the Eq.(25) exact analytical SS solution and the COMSOL solution of Eqs.(7a-b). Figures(5c-d) show the effect of turning on the $\mathbf{E}'_x$ field for two β parameters. Figures(6a-d) show the Ψ_1,Ψ_4 solutions vs x′

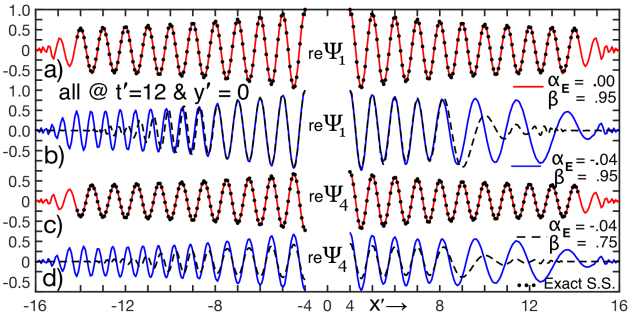

Figure 6. Ψ_1,Ψ_4 vs x′ @ y′=0 at Fig.(4) Section cuts

for line cuts at y′=0. Agreement is good between the SS exact and FEM solutions in Figs.(6a&c). Like the Bar, Figs.(6b&d) show the CylW part propagating in x′< 0 ($\mathbf{E}'_x$ direction) compresses and the part propagating in x′ > 0 (opposite $\mathbf{E}'_x$ direction) expands.

4.3 Two Slit Interference Example in Φ′ Field

A 2-D semi circular disk, of radius R′$_o$=40.0

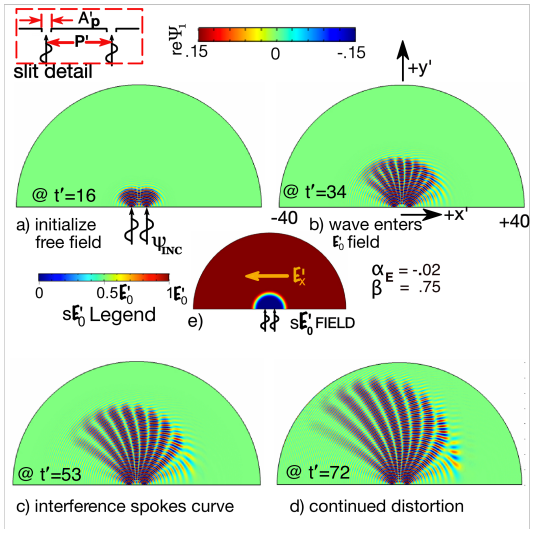

Figure 7 Transient Two Slit *Transverse* $\mathbf{E}'_x$ Field

FEM model consist of 2 slits of aperture A′$_p$=0.6 and separation P′=5.0 that are embedded in a baffle as shown in the Fig.(7) "*slit detail*" inset.

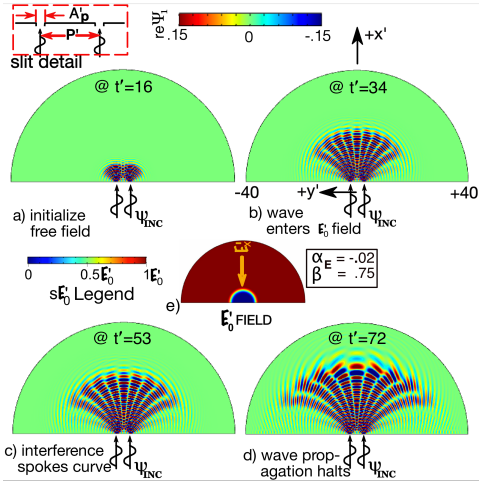

Figure 8 Transient Two Slit *Inline* $\mathbf{E}'_x$ Field

A (*ii*) zero value B.C. is used downfield on the curved surface. It is assumed that the probability of the particle appearing on the back slit wall is negligible so the (*ii*) zero value B.C. is also used there. The media consist

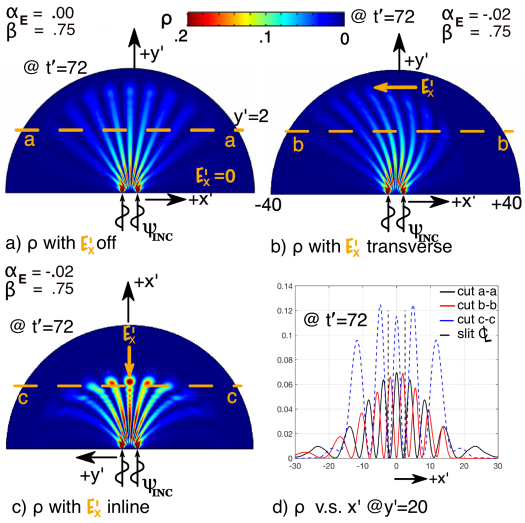

Figure 9 $\mathbf{E}'_x$ Field On vs. Off Comparisons of ρ

of an existing Eq.(8a-b) transverse electric field bounded upfield by a circular sector of free field in vacuo media that just encloses the slits as shown in Fig.(7e). Like the previous example, the electric field value $s(r'-r'_o)*\mathbf{E}'_0$ is turned on gradually by multiplying it by the COMSOL ∫ transition step function with a radial argument (e.g. Fig.(7e)). The slit openings are uniformly driven with the same driver used in the **4.1** bar models. The

$re\Psi_1(x',y',t')$ time history evolvement for a *transverse* and *inline* $\mathcal{E}'_x$ orientation at four time snapshots, is shown respectively in Figs.(7a-d) and Figs.(8a-d). The wave appears to halt propagating radially between Fig.(8c) and (8d), where stoppage alines with the x′ point at which $k^{2\prime}_{\phi}$ in Eq.(10a) turns negative. The probability density ρ, at t′=72 both with electric field turned on vs off, is shown in Fig.(9a-c). The "$\mathcal{E}'_x$ off" straight spoke interference patterns of Fig.(9a) are in contrast to the curved spoke interference patterns of Figs.(9b-c). The Fig. (9d) line plots (at cut planes a-a, b-b, and c-c), nicely illustrate the constructive-destructive interference patterns.

5. Magnetic Potential $\bar{A}'$ Field Alone ($\Phi'=0$) Results

The same problems addressed in section **4.1** and **4.3** are resolved using the Eqs(12a-b) magnetic $\bar{A}'$ field (with $\Phi'=0$). Both the temporal surface driver and magnetic field spatial distribution are gradually applied as in **4.0**.

5.1 Bar Plane Wave Guide in $\bar{A}'$ Field

First order form Eqs.(4a-b) were used to generate the Fig.(10) solution (e.g., in contrast to Eqs.(11a-b)), because they integrated over longer times before having integration problems (see **6.**). In this example we have an exact solution for validation, where FEM agreement was good as in Figs. (10d-g). The Ref.[3] SS uncoupled version of Eqs.

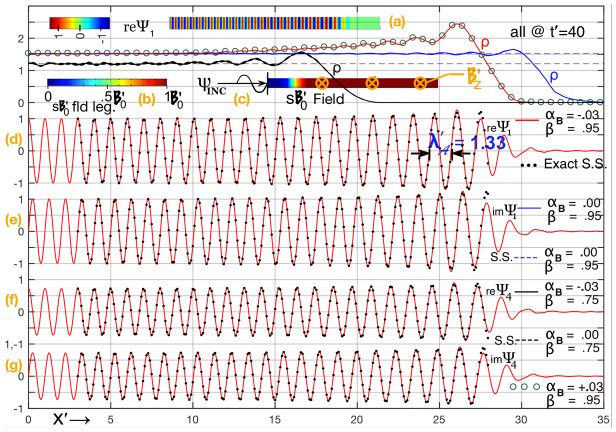

Figure 10. PW Passes Thru (α_B = -0.04) $\bar{A}'$ Field

(11a-b) reduces to the ode $d^2\psi_1/dx'^2 + (a\text{-}bx'^2)\psi_1=0$ which was solved symbolically with Mathematica™. The exact solution is $\psi_1(x\ w')=P_{CD}[\hat{a},-i\hat{b}x']/P_{CD}(\hat{a}, 0]$,where here $P_{CD}[\_,\_]$ is the two argument "ParabolicCylinderD" function (as defined in Mathematica™) where $\hat{a}=(-a-\sqrt{b})/(2\sqrt{b})$; $\hat{b}=\sqrt{2}\sqrt[4]{b}$. The wave length (e.g. using Eq.(13b) evaluated @ the mid point x′=25.02 between nulls) is approximated with $\lambda'_A \approx 2\pi/k'_A = 1.34$ as compared to the Fig.(10d) 1.33 graphical measurement.

5.2 Two Slit Interference Example in $\bar{A}'$ Field

Second order form Eqs.(11a-b) were used to generate the Fig(11) solution. The Fig.(11b) interference

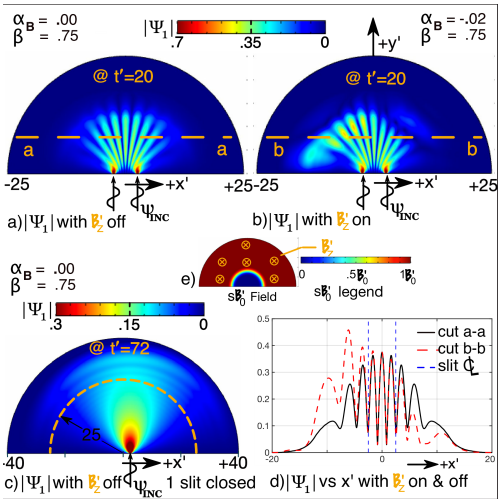

Figure 11. Transient Two Slit $\bar{A}'$ Field

spokes are curved by the $\mathcal{B}'_z$ magnetic "*field on*" in contrast to the Fig.(11a) "*field off*" straight ones. The Fig.(11c) interference spokes disappear with one slit closed.

6. Concluding Remarks

An uncoupled, better converging second order PDE version of the Magnetic field alone Eqs.(11a-b) is obtained by eliminating the $\partial\Psi_4'/\partial t'$ in Eq. (11a) with Eq.(4b) and eliminating the $\partial\Psi_1'/\partial t'$ in Eq.(11b) with Eq.(4a). Based on preliminary computations with these reduced PDE's (using alternate FEM code Mathematica™), improved stability and convergence characteristics over longer time integration ranges were experienced (e.g. Fig. (10d-g) was reproduced. The same improved performance using COMSOL is anticipated.

7. References

[1] A.J. Kalinowski,"Relativistic Quantum Dirac … Equation", COMSOL Conf. Proc., 2016.

[2] A.J. Kalinowski,"Time Dependent Dirac … Mechanics", COMSOL Conf. Proc., 2017.

[3] A.J. Kalinowski,"Relativistic Quantum Mechanical … Magnetic Fields", COMSOL Conf. Proc. 2018.

[4] Paul Strange, Relativistic Quantum Mechanics, Camb. Univ. Press Cambridge 1998.